Asymmetric Hard Domain-Induced Self-Healable Waterborne Polyurethane

Highlights

Inspired by the mussel byssus cuticle, an asymmetric alicyclic architecture viz. isophorone diisocyanate- isophorone diamine (IPDI-IPDA) moiety was introduced into the hard domain of the waterborne polyurethane (WPU) matrix to develop a series of transparent, elastomeric shape memory-assisted self-healable biobased WPU with unprecedented toughness, extreme stretchability, high fracture energy, reprocessability, biocompatibility, and biodegradability for biomedical applications. These outcomes can be attributed to high-density hindered urea-based hydrogen bonds originating from the IPDI-IPDA system and chemical cross-linking based on glycerol ester of citric acid (GECA). Most importantly, platelet adhesion study, lactate dehydrogenase (LDH) activity, and erythrocyte or red blood corpuscle (RBC) lysis demonstrated the hemocompatibility of the developed elastomer. Simultaneously, cellular viability (live/dead) assay and cell proliferation (Alamar blue) assay of human dermal fibroblasts (HDFs) corroborated the biocompatibility under in vitro conditions. Furthermore, the synthesized WPU showed melt reprocessability and microbial-assisted biodegradation. Overall results, therefore, indicate that the developed WPU elastomer might be used as a potential smart biomaterial (e.g., suture) and coating for biomedical devices.

Parts of this chapter are published in

Morang, S., Bandyopadhyay, A., Mandal, B.B. and Karak, N. Asymmetric hard domain-induced robust resilient biocompatible self-healable waterborne polyurethane for biomedical applications. *ACS Applied Bio Materials*, 6(7):2771-2784, 2023. (DOI: 10.1021/acsabm.3c00243)

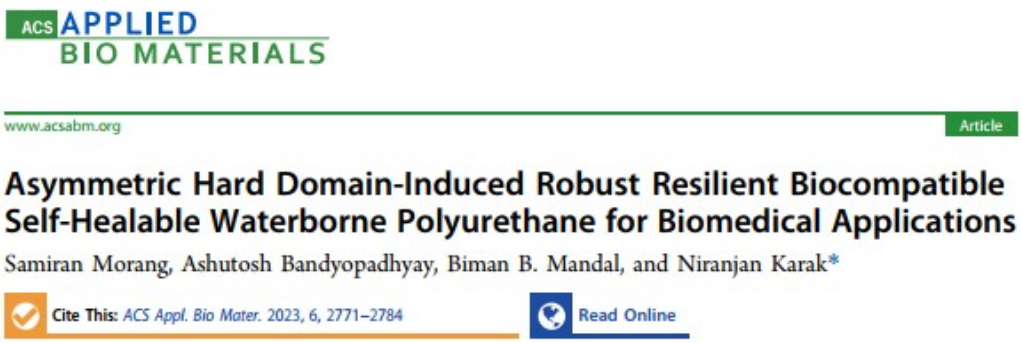

4.1. Introduction

From the **chapter 3** it is observed that self-healable poly(urethane/acrylic) (SWPUA) hybrid films exhibited microwave assisted self-healing (SH) and melt reprocessable attributes in addition to other common properties. Interestingly, hybrid dispersions can also be used for 3D-bioprinting. However, mechanical properties of those hybrid films are not suitable for advanced applications and dispersions is safe to use only up to 30% for *in vitro* conditions. Therefore, pristine WPU needs to be modified further to improve their performance and biocompatibility.

From **Chapter 1**, it is comprehensible that WPU have tunable mechanical properties which can be tuned via alternating the "hard" to "soft" segment ratio i.e., controlling the microphase-separated structure of the WPU [1]. This structure analog with the soft and hard components of mussel byssus cuticle that shows an unparalleled combination of high mechanical strength, stretchability, toughness, and self-healing ability. The outcome can be accredited to the exclusive architecture of granular crosslinks with Fe^{3+}, which coordinates dopamine dispersion in the nearby soft protein matrix [2-3]. This structural relationship raises the ray of hope to integrate seemingly paradoxical properties i.e. high mechanical strength and SH ability into one elastomer by designing its microphase-separated architectures, precisely. Again, literature advocates that intrinsic self-healing can be introduced in WPU matrix via non-covalent bonds such as hydrogen bonds [4-5], metal-ligand [6], host-guest interactions [7] and covalent bonds formation through Diels-Alder [8], radical recombination [9], hidden urea bond [10], olefin metathesis [11], boronic esters [12], and so forth. Strong multiple hydrogen bonds present in the hard domains are extensively used for the production of intrinsic self-healing PU because of their versatile, directional, and reversible nature [13]. The reversible dissociation and re-association of H-bonds facilitate the molecular chain mobility and hence self-healed the damaged surface with or without any stimuli [14].

In this work, we have mimicked mussel byssus cuticle structure to synthesize a transparent self-healable WPU elastomer with unprecedented toughness, extremely high stretchability multi-stimuli (heat, microwave radiation, and sunlight) responsive shape memory, reprocessability, and biodegradability attributes via the synergistic effect of strong reversible physical and chemical crosslinking. The asymmetric isophorone diisocyanate (IPDI) and isophorone diamine (IPDA) generate the asymmetric IPDI-IPDA moieties, resulting loosely packed hard domain and create seemly network for healing. Simultaneously, the chemical cross-linker glycerol ester of citric acid (GECA) and the self-

flexible poly(ε-caprolactone diol) (ε-PCL_{2000}) facilitate shape recovery ability which also assist to repair the damaged area of the WPU elastomers. Most importantly, platelet adhesion study, lactate dehydrogenase (LDH) activity, and erythrocyte or red blood corpuscle (RBC) lysis demonstrated the hemocompatibility of the developed elastomers. Consequently, cellular viability (live/dead) assay and cell proliferation (Alamar blue) assay using human dermal fibroblasts (HDFs) seeded on the elastomers corroborated the biocompatibility under *in vitro* conditions. So, the novel biocompatible high-performance WPU elastomers can potentially be used in minimally invasive smart biomedical devices (e.g. suture) and in wearable electronics.

4.2. Experimental

4.2.1. Materials

Raw material used in this work are IPDI, ε-PCL_{2000}, 2,2-bis(hydroxymethyl) propionic acid (DMPA), citric acid, glycerol, castor oil, triethyl amine (TEA), *para*-toluene sulphonic acid (*p*-TSA), calcium oxide (CaO), 1,6-diaminohexane (HMDA), N, N-dimethylformamide (DMF), and dibutyltin dilaurate (DBTDL) have the same specifications and grades as stated in the **Chapter 3**, **Section 3.2.1**.

IPDA is a colorless liquid with a molecular weight of 170.3 $gmol^{-1}$, density of 0.92 gmL^{-1}, and boiling point of 247 °C. It was used as a chain extender to prepare WPU.

4.2.2. Methods

4.2.2.1. Preparation of monoglyceride of castor oil (MG_{CO})

The biobased chain extender monoglyceride of castor oil (MG_{CO}) was prepared by glycerolysis of ester as discussed in **Chapter 2**, **section 2.2.2.1**.

4.2.2.2. Preparation of glycerol ester of citric acid (GECA)

GECA was prepared by an esterification reaction as described in **Chapter 2**, **section 2.2.2.2**.

4.2.2.3. Preparation of biobased waterborne polyurethane (WPU)

The chemical compositions of the five WPUs are presented in **Table 4.1**. The molar ratio of isocyanate (-NCO) to hydroxyl (-OH) functionality was maintained at 1. The synthesis procedure of WPUs involves the following steps. In the first step, a stoichiometric amount of ε-PCL_{2000} (3g, 1.5 mmol), DMPA (0.201 g, 1.5 mmol), and IPDI (0.76 mL, 3.6 mmol), along with DBTDL (0.0025 g) were added to a 100 mL three neck round bottom flask reactor equipped with a mechanical stirrer, a nitrogen inlet, and a stopper. The mixture was reacted

for 2.5-3 h at 70-80 ℃ to prepare a linear NCO-terminated prepolymer. In the second step, the calculated amount of MG_{CO}, GECA, and remaining IPDI were added to the reaction mixture and heating was continued for another 4-5 h at the same temperature.

Table 4.1. Chemical compositions of the reactants for preparing WPUs.

Reactants	WPU-H (mM)	WPU-HI-1 (mM)	WPU-HI-2 (mM)	WPU-HI-3 (mM)	WPU-I (mM)
ε-PCL	1.5	1.5	1.5	1.5	1.5
DMPA	1.5	1.5	1.5	1.5	1.5
MG_{CO}	1	1	1	1	1
GECA	0.375	0.375	0.375	0.375	0.375
HMDA	0.35	0.263	0.175	0.088	0
IPDA	0	0.088	0.175	0.263	0.35
IPDI	5.6	5.6	5.6	5.6	5.6

In the next step, the free carboxylic acid groups were neutralized by TEA and dispersion was obtained by adding water and vigorous stirring at 850 RPM. Finally, the chain extension reaction was performed for 2h at 70-80 ℃ to obtain the desired WPU dispersion. This dispersion was further cast on a Teflon sheet and the films were utilized for various analyses and tests.

4.2.3 Characterization and tests

4.2.3.1. Structural characterization and property evaluation

Various analytical techniques and tests were adopted for the characterization and evaluation innate properties of WPUs dispersion and their films as described in **Chapter 2** and **Chapter 3**. Furthermore, stress–relaxation tests was performed using a dynamic mechanical analyzer (DMA, Anton Paar, Model-MCR702. The samples were subject to a fixed strain of 10% for a relaxation time of 15 min at different condition. Rectangular specimens with dimensions of 20 mm × 3 mm × 0.3 mm were used for the test.

4.2.3.2. Fracture test

Resistance to the fracture was scrutinized from the stress-strain profile of the single-edge notched sample (length of the notch is 1mm) and un-notched sample (length × width × thickness:: 50 mm × 5 mm × 0.76 mm). The rate of displacement was fixed at 20 mmmin^{-1} for both specimens. The fracture energy (G_c) was calculated from the Greensmith Method using the following equation [15-16].

$$G_c = \frac{6Wc}{\sqrt{\lambda_c}} \qquad \textbf{Eq. 4. 1}$$

Where c designates notch length; W designates the strain energy measured via integrating the stress-strain curve of an un-notched sample until λ_c.

4.2.3.3. Self-healing, shape memory, and re-processability tests

The quantitative evaluation of SH ability of WPU was carried out as reported in **Chapter 3**. Additionally, 0.1-0.2 µL of DMF was dropped on the damaged area, and the two pieces of WPU film were contacted gently. Then, the trace solvent was removed by a normal saloon hair drier followed by drying the specimens inside a convection oven at 90 ℃ for 2 h.

To investigate the shape memory behaviors, films were temporarily shaped into ring and spiral shapes at 60 ℃ (T_g + approx. 20 ℃) for 5 min. Then, the films were immediately plunged into an ice-water salt bath at -5 ℃ for 10-15 min and placed inside a vacuum oven at room temperature. The vacuum-dried films were tested for shape recovery and shape fixity in the presence of heat, microwave, and sunlight, using the following equations.

$$\text{Shape fixity } (\%) = \frac{\theta}{90} \times 100 \qquad \textbf{Eq. 4. 2}$$

$$\text{Shape recovery } (\%) = \frac{90 - \theta}{90} \times 100 \qquad \textbf{Eq. 4. 3}$$

Where θ refers to the angle formed between the tangent at the middle point of the specimen and the line that connects the middle point and the edge of the ring or spiral shape.

Furthermore, the re-processability of WPU films was performed using a compression-molding machine as mention in **Chapter 3**.

4.2.3.4. *In vitro* hemocompatibility study

4.2.3.4.1. Platelet adhesion study and lactate dehydrogenase (LDH) activity

Goat whole blood was received from the healthy animals from the local abattoir in a centrifuge tube containing heparin (5 Uml^{-1}, Sigma Aldrich, USA). This blood was centrifuged

at 3000 rpm for 10 min at 22 °C and the platelet rich yellowish top layer of plasma (PRP) was obtained. *In vitro* hemocompatibility and anti-thrombogenic ability of WPU films were assessed using the previously described protocols by observing the number of adhered platelets and the activity of these platelets using LDH assay [17]. Disks (ϕ 5 mm) of various WPU films namely WPU-H, WPU-HI-1, WPU-HI-2, WPU-HI-3, and WPU-I were incubated with 200 µL of PRP at room temperature (RT) for a duration of 1h. Surfaces coated with collagen (3 mg ml^{-1}, Sigma Aldrich, USA) were taken as the positive control. All disks were washed twice with PBS (pH 7.4) post incubation and fixed using neutral buffered formalin (NBF, Sigma Aldrich, USA). The disks were further treated with 0.1% (v/v) TritonX-100 (Sigma Aldrich, USA) to permeabilize the adhered platelets for 15 min at RT and fluorescently labelled with rhodamine-phalloidin (1:40, Life Technologies, USA) to observed under the inverted fluorescence microscope (Nikon Eclipse Ti-2, Nikon, Japan).

Additionally, the activity of the adhered platelets was quantified using LDH assay as mentioned in previously described protocols. Herein, disks (n=3) were incubated with 200 µL of PRP along with collagen coated control surfaces for 1h at RT. Thereafter, the adhered platelets were subjected to lysis using 1% TritonX-100 for 1 h at 37 °C. The hence collected platelet lysate was centrifuged at 10000 rpm at 4 °C for 10 min and the supernatant was used to measure LDH activity using a LDH kit (Sigma Aldrich, USA) and expressed in the form of milli units'(ml^{-1}). The LDH activity was directly correlated with the number of adhered and active platelets.

4.2.3.4.2. Erythrocyte lysis assay

Erythrocyte or red blood corpuscle (RBC) lysis induced by the various WPU films was determined as mentioned in previously described protocol [18]. Whole blood was collected and processed as described above and the bottom RBC containing layer was taken and washed with 150 mM NaCl buffer twice and repeatedly centrifuged. Washed RBC containing blood was 20x diluted with 150 mM NaCl buffer for experimental purposes. The various WPU disks (ϕ 5 mm) were incubated (n=3) with 200 µL of diluted RBC containing blood for 1 h along with 20% triton X-100 (Sigma Aldrich, USA) and 150 mM NaCl buffer as positive (n=3) and negative (n=3) controls, respectively. The incubated blood was collected, and intact RBCs were centrifuged down at 3000 rpm for 5 min and the supernatant was read at 540 nm in a Multiskan Sky multiplate reader (Thermo Scientific, USA). The obtained absorbance was correlated with the RBC lysis potential and plotted.

4.2.3.5. *In vitro* degradation study

The WPU films were subject to incubation in 0.1M PBS at 37 °C in a shaking incubator set at 30 rpm over a period of 60 days according to the ASTM standard method described previously [17]. WPU films were maintained in a film to PBS weight ratio of 1:3 and the weight was measured for these films after 15, 30, 45, and 60 days of incubation post washing with deionized water and drying at 37 °C. Mass loss percentage was calculated using the below-mentioned equation.

$$\text{Degradation weight (\%)} = \frac{W_1 - W_i}{W_i} \times 100 \qquad \textbf{Eq. 4. 4}$$

where, W_i is the initial dry weight of the film and W_1 is the dry weight of the film at various time points.

4.2.3.6. *In vitro* cytocompatibility and cell proliferation study

WPU films were evaluated for their cytocompatibility *in vitro* using human dermal fibroblasts (HDFs) using cell viability (live/dead) assay and cell proliferation (Alamar blue) assay for a period of 7 days as described previously [19]. HDFs were cultured in complete medium of DMEM (Gibco, USA) containing 10% fetal bovine serum (FBS, Gibco, USA) and 1% antibiotic-antimycotic solution (Himedia, India). WPU films (5 × 5) mm were sterilized using ethanol (70% v/v), washed with PBS and preconditioned in a complete medium for 24 h pre-seeding. Confluent HDFs were trypsinized and suspended in complete medium and seeded on the WPU films as well as tissue culture plate (TCP) control. Cell viability post 7 days of seeding was checked using live/dead assay as per manufacturer's protocol. Briefly, the cell seeded films were washed with PBS and incubated with a solution of 4 mM calcein AM (for live cells) and 2 mM ethidium homodimer (for dead cells) (Sigma Aldrich, USA) for 20 min at 37 °C in humidified incubator. The films were washed with PBS post staining and cells were imaged using inverted fluorescence microscope (Nikon Eclipse Ti-2, Nikon, Japan).

Similarly, HDFs were seeded onto various WPU films (n=4) and TCP (~$2x10^4$ cells) (n=3) and their proliferation was observed at 1, 3, 5 and 7 days using Alamar blue assay (Invitrogen, USA) according to manufacturer's protocol. In brief, the seeded films were incubated in complete medium containing 10% (v/v) Alamar blue dye at 37 °C in a 5% CO_2 incubator for 3 h. The absorbance of the media containing reduced alamar blue dye was measured at 570/600 nm using Multiskan Sky multiplate reader (Thermo Scientific, USA).

4.2.3.7. Biodegradation test

The biodegradability of WPUs film was investigated using the McFarland turbidity method in an incubator by introducing a *B. subtilis*, as stated in **Chapter 2**.

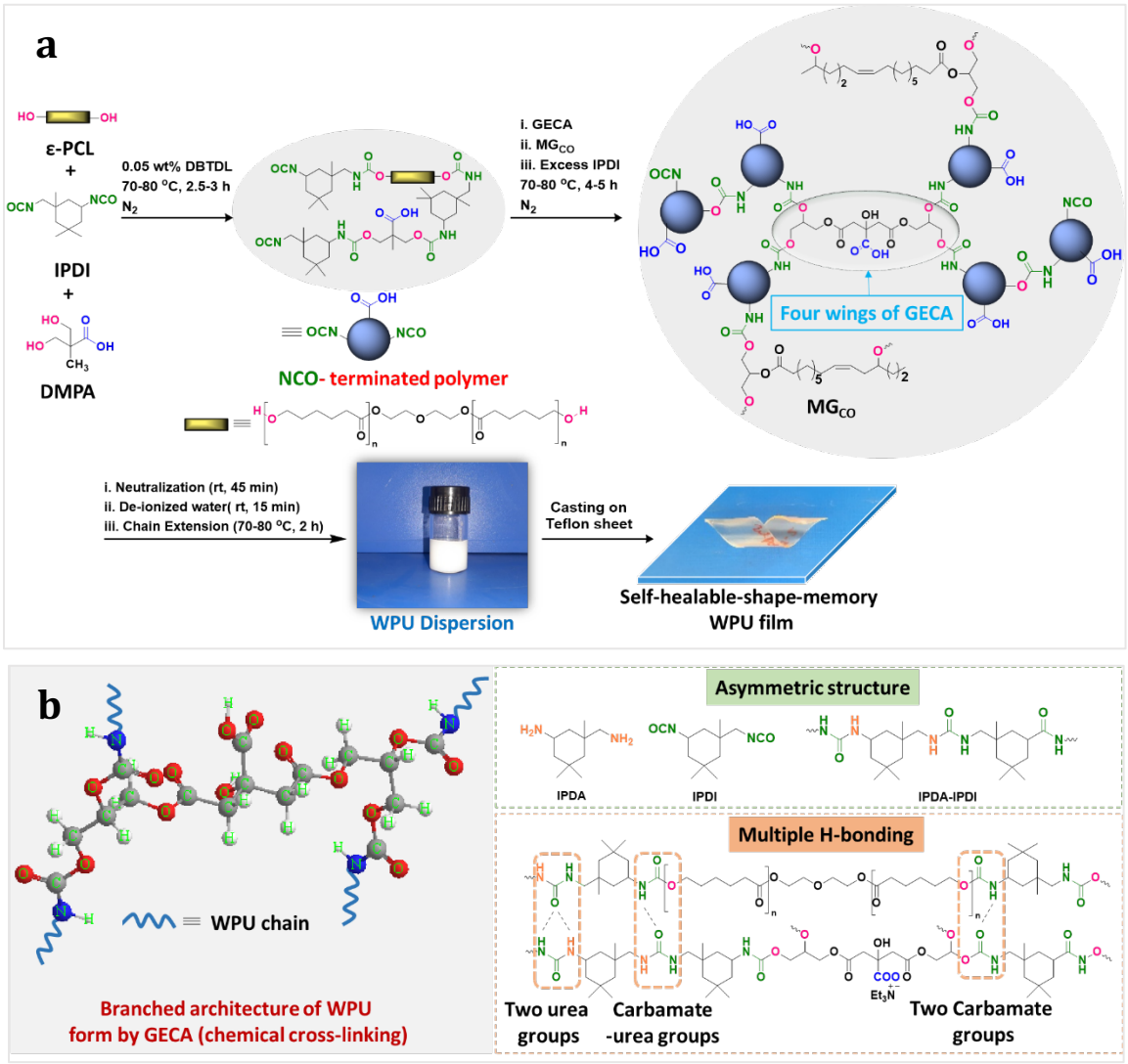

Scheme 4.1. (a) Synthetic routes to WPU elastomers and (b) cross-linked structure of GECA and possible strong H-bonds developed between various groups (two urea groups, carbamate-urea groups, and two carbamate groups).

4.3. Results and discussion

4.3.1. Preparation and characterization of shape memory WPU

Here, a series of WPUs were prepared by pre-polymerization technique with different ratios of IPDA and HMDA, as shown in **Scheme 4.1**. The formation of the NCO-terminated prepolymer was confirmed by the FTIR peak at 2259 cm^{-1} corresponding to -N=C=O stretching as shown in **Figure 4.1**. Noticeably, the same peak is missing in the FTIR spectra of WPUs which further confirmed that there is no free isocyanate group. This zero isocyanate claims the conversion of free isocyanate groups into either urethane or urea linkage of the final product. The broad peak of the free -OH group which was found to be near 3500 cm^{-1}

was also absent but another broad peak was observed near 3452 cm^{-1} corresponding to -NH stretching frequency.

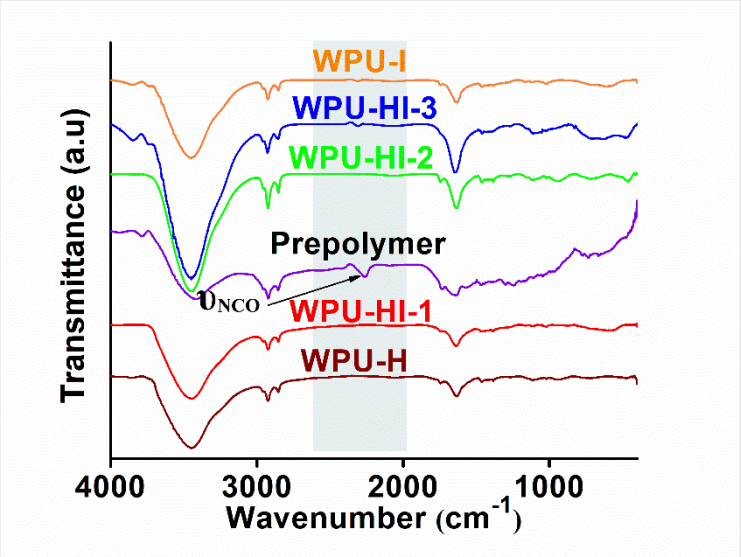

Figure 4.1. FTIR spectra of NCO-terminated prepolymer and WPUs.

A small peak at 1465 cm^{-1} can be accredited to the -NH bending vibration. Asymmetric and symmetric stretching frequency of $-CH_2$ groups were present at 2925 cm^{-1} and 2850 cm^{-1}, respectively. The characteristic peaks at 1742 cm^{-1} and 1639 cm^{-1} can be assigned to the C=O group of urethane linkages and urea linkages, respectively. Furthermore, a medium peak at 1381 cm^{-1} can be accredited to -CH bending vibrations. All these characteristic peaks point towards the formation of urethane linkage. The proposed chemical structure of WPU-HI-1 was confirmed by ^{1}H and ^{13}C NMR spectral analyses. In **Figure 4.2 (a)**, the chemical shifts near δ=0.86 ppm and δ=0.91 ppm (a, b; $-CH_3$) appear due to the presence of methyl protons of IPDI and IPDA. The peaks at δ=1.26 ppm, 1.27 ppm, 1.29 ppm, 1.30 ppm, and 1.32 ppm (d, $-CH_2$) can be assigned to the γ-methylene protons with respect to the ester groups and urea groups. Another five peaks located at δ= 1.49 ppm, 1.51 ppm, 1.52 ppm, 1.54 ppm, and 1.56 ppm (e, $-CH_2$) due to the presence of β-methylene protons with respect to the urea groups. Methylene protons adjacent to C-atom of the ester group present in GECA moiety appeared at δ 2.09 ppm (f, $-CH_2$) and that of present in ε-PCL_{2000} moiety appeared at δ= 2.25 ppm, 2.26 ppm, and 2.28 ppm (g, CH_2). The small peaks at δ= 2.64 ppm, 2.70 ppm, and 2.78 ppm (h, $-CH_2$) can be assigned to the α-methylene protons with respect to the urea groups. Three sharp peaks appeared at δ= 3.96 ppm, 3.98 ppm, and 3.99 ppm, correspond to the methylene protons nearby the O atom of urethane linkage. Methine protons of MG_{CO} moiety were observed at δ= 5.31 ppm, 5.39 ppm, 5.55 ppm, and 5.65 ppm (j, -CH). Three peaks located at δ= 5.74 ppm, 5.84 ppm, and 5.92 ppm (k, -NH) and δ= 6.91 ppm,

7.04 ppm, and 7.14 ppm can be accredited to the protons attached with the N-atom of urea linkage and urethane linkage, respectively.

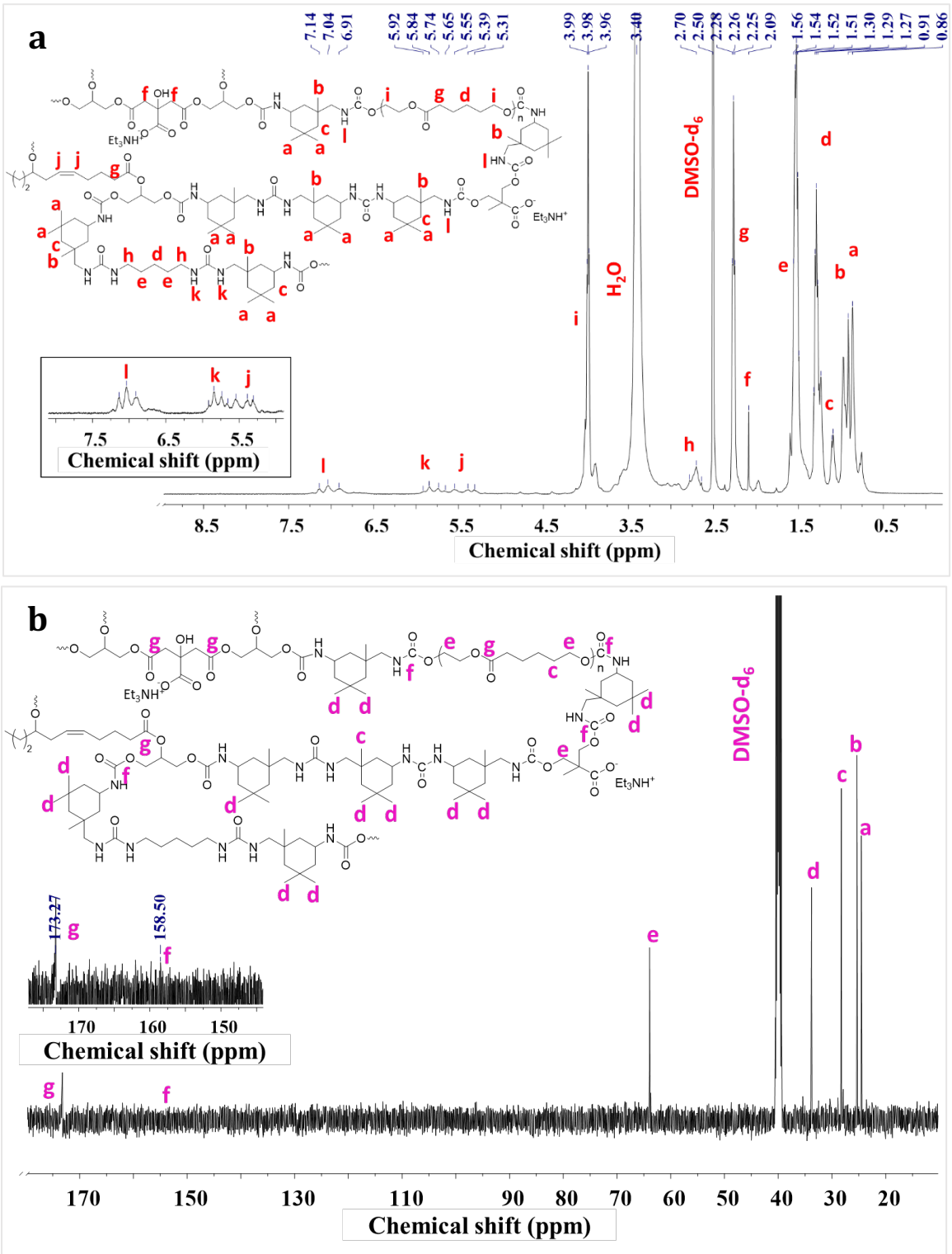

Figure 4.2. (a) ^{1}H NMR and (b) ^{13}C NMR spectra of WPU-HI-2.

Again, a perusal of ^{13}C NMR spectrum of WPU-HI-1 (**Figure 4.2 (b)**) indicated that the presence of peaks at δ= 24.53 ppm (a) and 25.34 ppm (b) which can be assigned to the γ-

carbon of urea and ester linkages, respectively. Free methyl carbons of IPDI and IPDA moieties appear at δ= 28.25 ppm (c) and 33.81 ppm (d).

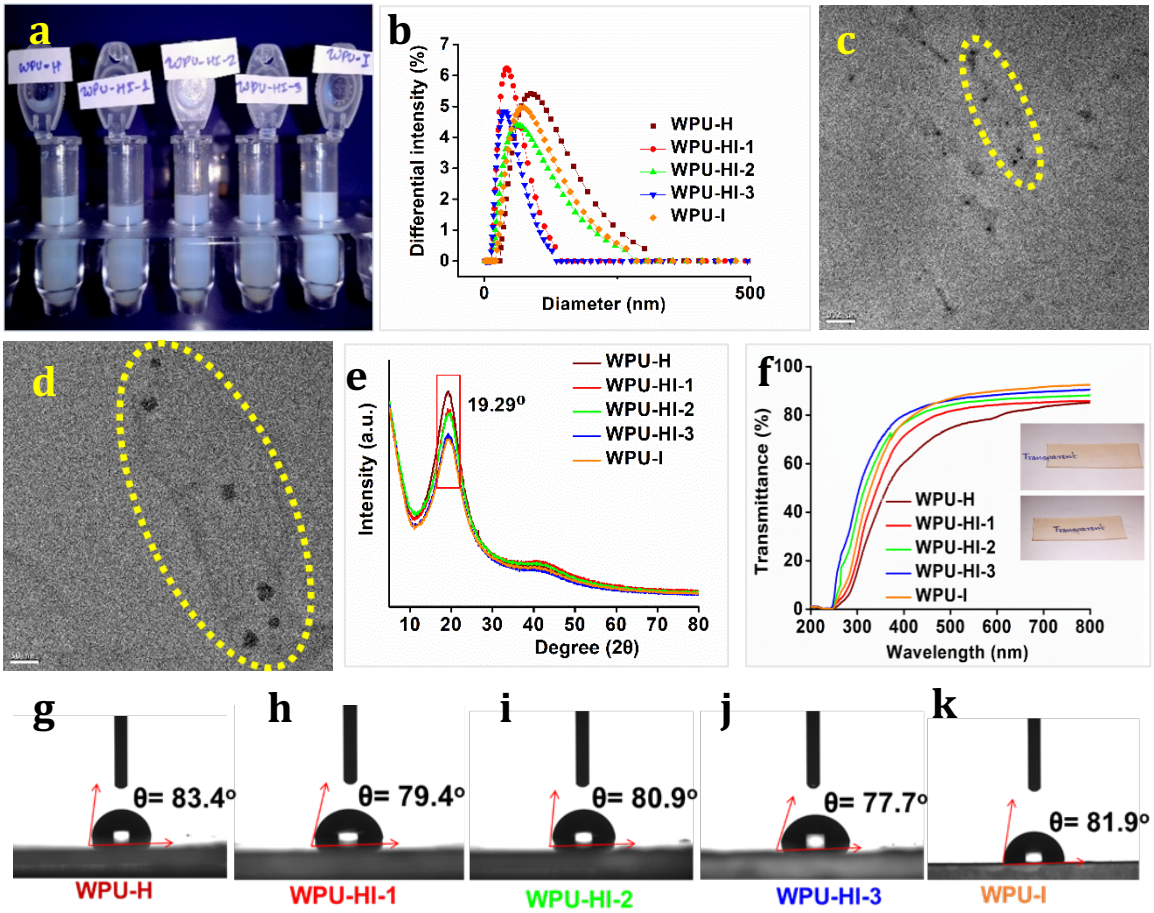

Figure 4.3. (a) Digital images of WPUs (at actual scale, 2.5 mL Eppendorf), (b) particle size distribution, (c-d) TEM images of WPU-HI-2 (0.2 μm, and 50 nm, (e) P-XRD spectra of WPUs, (f) percentage of transmittance of WPU films of thickness 0.10 mm, in set: The word "**transparent**" can be easily visible through the WPU-HI-2 film (thickness 0.10 mm), and (g-k) water contact angle of WPUs.

A sharp peak observed at δ= 63.94 ppm (e) can be accredited to the methyl carbon attached with the O atom of urethane linkage. Again, the peak corresponding to carbonyl carbon of ester and carbamate groups appeared at δ= 173.27 ppm and 158.50 ppm, respectively. All these results support the proposed structure of the WPU-HI-1. Molecular weights of WPUs are very close to each other as similar polymerization condition was followed. Weight average molecular weight of WPU-H, WPU-HI-1, WPHU-HI-2, WPU-HI-3, and WPU-I were 43852 $gmol^{-1}$, 51947 $gmol^{-1}$, 56603 $gmol^{-1}$, 51193 $gmol^{-1}$, and 40832 $gmol^{-1}$, respectively. The digital images and particle size distributions of the prepared WPUs were shown in **Figure 4.2 (a)** and **(b)**. The average particle sizes of the WPU-H, WPU-HI-1, WPU-HI-2, WPU-HI-3, and WPU-I were 104.4 nm, 71.8 nm, 77.2 nm, 44.7 nm, 87.4 nm, respectively with low particle distribution indexes in the range of 0.193 to 0.221. TEM images also

support the small particle size, as shown in **Figure 4.3 (c)** and **(d)**. Generally, two factors control the particle size and stability of WPUs, namely, the amount of cross-linker (functionality, f ≥ 3) and emulsifier loaded into the WPU system, as stated in the earlier chapter. In this study, all WPUs have very close particle size distribution as all compositions contain the same amount of DMPA and GECA. The dispersions were stable for up to three months. The crystallinity of the WPUs films was investigated at 2θ ranging from 5° to 80°, as shown in **Figure 4.3 (e)**. In this work, the semi-crystalline ε-PCL_{2000} was used as the macroglycol which exhibits two characteristic peaks at 2θ= 21.4° and 23.8° corresponding to (110) and (200) reflection plans [20]. However, the crystallinity was not retained after polymerization because of crosslinking which restricts the chain mobility or entanglement resulting in WPUs. It has been observed that there is a broad peak near 19.29° for all compositions which can be accredited to the soft semi-crystalline segment i.e., ε-PCL_{2000}. The peak intensity decreased from WPU-H to WPU-I with the increase in the content of asymmetric chain extender IPDA showing the development of more amorphous phases. The transparency of the WPU films was measured using a UV-visible spectrophotometer. **Figure 4.3. (f)** showed that the films are sufficiently transparent to see the word **transparent** covered by WPU-HI-2 film of thickness 0.10 mm. It can be observed that the transparency order is WPU-I (91.48%) > WPU-HI-1 (90.9%) > WPU-HI-2 (88.05%) > WPU-HI-3 (85.34%) > WPU-H (80.57%). This can be attributed to the decrease in the crystallinity in the WPU films with increase in the loosely packed hard domains formed by IPDA-IPDI moieties. The surface hydrophilicity of the WPU films was investigated by measuring the water contact angle. As shown in **Figure 4.3. (g-k)**, the water contact angles of WPU-H, WPU-HI-1, WPU-HI-2, WPU-HI-3, and WPU-I films were 83.4°, 81.9°, 79.4°, 80.9°, and 77.7°. DMPA and GECA act as the hydrophilic moieties which provide free carboxylic acid groups to develop ionic interactions with TEA. So, all the films are hydrophilic in nature.

4.3.2. Thermal properties WPUs

To evaluate the thermal properties of WPU films, TGA and DSC analyses were performed and the results are presented in **Figure 4.4**. The thermal stability of WPU is influenced by several factors such as the percentage of cross-linked moieties, the ratio of hard to soft segments, rigid moiety (e.g., benzene ring and other rings), and molecular weight of the resulting WPUs. From the TGA and DTG curves (**Figure 4.4 (a)** and **(b)**), it can be seen that there are two steps in the degradation of the WPU films in the range of 332-338 °C and 435-441°C which are similar to the prior literature reports [21]. The first step degradation can be attributed to the relatively thermo-labile groups such as urethane linkages, urea linkages, and long

aliphatic hydrocarbon chains of MG_{CO}, HMDA, and GECA. On the other hand, the thermostable moiety such as aliphatic rings of IPDI and IPDA was degraded in the second step. It can be seen that the order of the thermal stability increases from WPU-H to WPU-I. This increment arises because of an increment in the content of the alicyclic moiety i.e., IPDA.

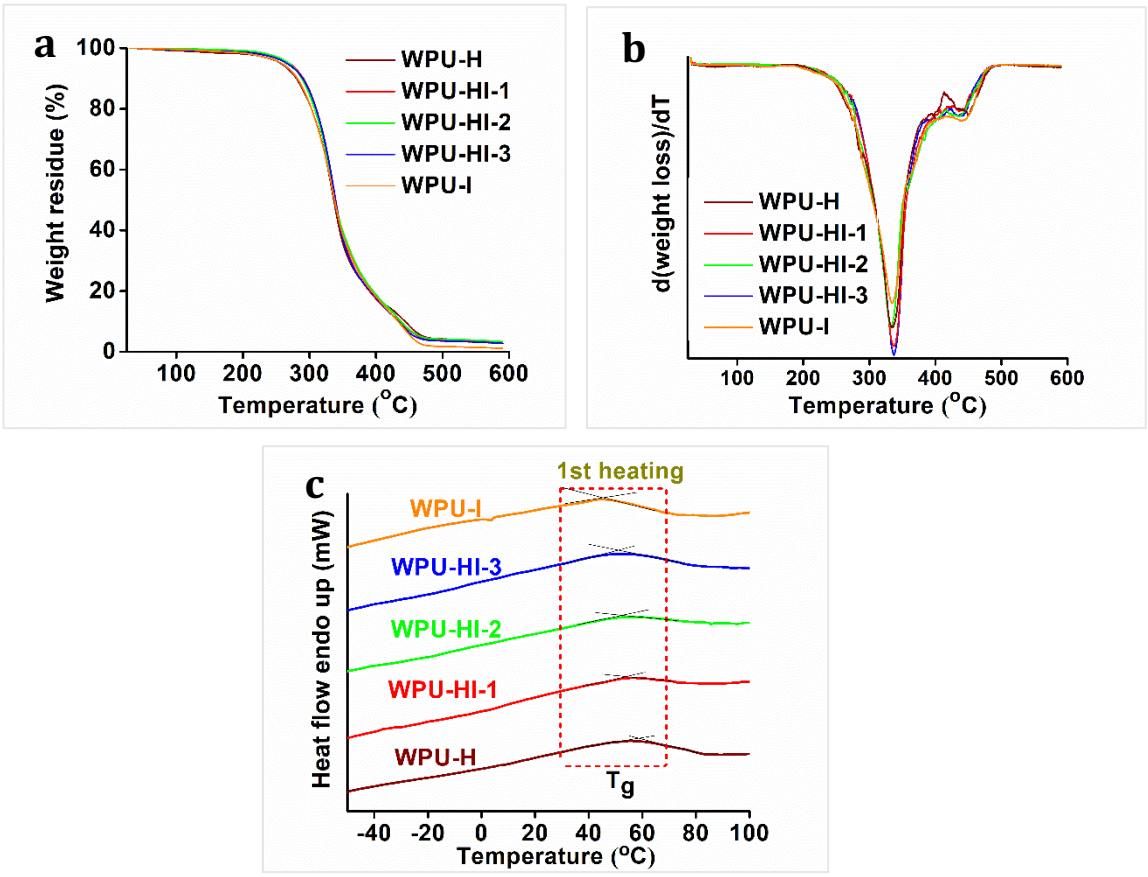

Figure 4.4. (a) TGA thermograms, (b) first order derivative curves (DTG), and (c) DSC curves of WPUs.

Furthermore, the glass transition temperature (T_g) of WPUs were determined from DSC curves and presented in **Figure 4.4 (c)**. Results showed that the T_g of hard segment of WPU-H, WPU-HI-1, WPU-HI-2, WPU-HI-3, and WPU-I were 55.9 °C, 54.7 °C, 54.1 °C, 51.4 °C, and 46.0 °C, respectively. An increase in the IPDA content from 0% to 100% resulted in a gradual decrease in T_g from 55.9 °C to 46.0 °C indicating the development of high degree of phase separation and hence the high mobility of molecular chains. This trend is also supported by the P-XRD data in which crystallinity decreases with an increase in IPDA amounts.

4.3.3. Mechanical performance WPU films

It can be seen from the stress-strain profiles that all WPUs exhibited high tensile strength and extreme flexibility (**Figure 4.5 (a-c)**). WPU-H demonstrated impressively the highest

strain of 6356±105.50% and tensile strength of 9.29±0.37 MPa. Again, the tensile strength and strain of WPU-HI-1, WPU-HI-2, WPU-HI-3, and WPU-I were found to be 13.07±0.19 MPa and 5419±100.15%, 13.85±0.43 MPa and 3714±122.56%, 15.25±0.15 MPa and 3395±151.73%, 15.84±0.57 MPa and 3297±190.68%, respectively.

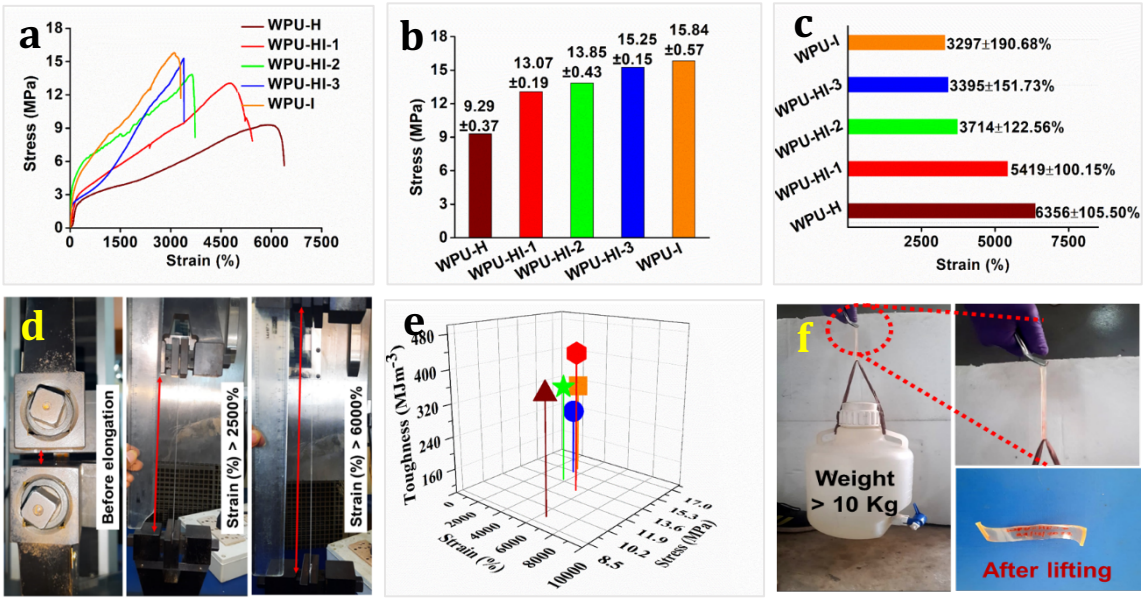

Figure 4.5. (a) Stress-strain profiles, (b) maximum stresses (MPa), (c) percentages of maximum strain at break of WPU films, (d) Digital images of stretchability (> 6000%) of WPU-H, (e) 3D-variations of toughness (MJm^{-3}), mechanical strength (MPa), and strain (%) of all WPU films, and (f) photograph demonstrate that WPU-HI-3 film (0.66 g) can lift more than 10 kg weight.

It is pertinent to note that the mechanical properties of WPUs depend on various factors such as structural coincidence, molecular weight, presence of rigid moieties, physical and chemical cross-linking through non-covalent and covalent interactions, and chain entanglement [7]. Results showed that the tensile strength of WPUs increases with the increase in the content of IPDA from 0 to 100%. The asymmetric and alicyclic structure of IPDA and IPDI results in the formation of the irregular repeating units of IPDA-IPDI which facilitate strong multiple H-bonds. The fabrication of the IPDA-IPDI moiety into PU backbone (PCL-IPDI) not only increases the percentage of hard domains but more importantly, also embeds irregularly arranged urea groups between adjacent soft ε-PCL moiety. Furthermore, four wings of GECA provide a positive contribution to the tensile strength increasing via chemical crosslinking by the formation of four urethane linkages with IPDI (showed four urethane bonds). Again, high flexibility is obtained due to the presence of long hydrocarbon chains in MG_{CO}, HMDA, and PCL moieties. As expected, the strain decreases with the increment in the IPDA content. The extremely high flexibility (6356%) of WPU-H is shown in **Figure 4.5 (d)**. Again, toughness is related to energy dissipation capacity, so it is directly

associated with tensile strength and stretchability. Though these two properties are contradictory to each other, the optimum outcome can be obtained by increasing dynamic noncovalent crosslinks which are provided in this work. The toughness of WPUs is shown in **Figure 4.5 (e).** Amazingly, the toughness of WPU-HI-1 was as high as 436.1 MJm^{-3}. This toughness can be considered as one of the highest reported values for self-healable polymer and even tougher than the renowned toughest spider silks across the globe [22-23]. Interestingly, a WPU-HI-3 specimen (0.657 g, 50 mm long, 10 mm wide, and 0.8 mm thickness) is able to lift a weight of 10 kg water container (with 10.3 L water,) which is 15,677 times greater than its own weight, successfully without any damage as shown in **Figure 4.5 (f)**.

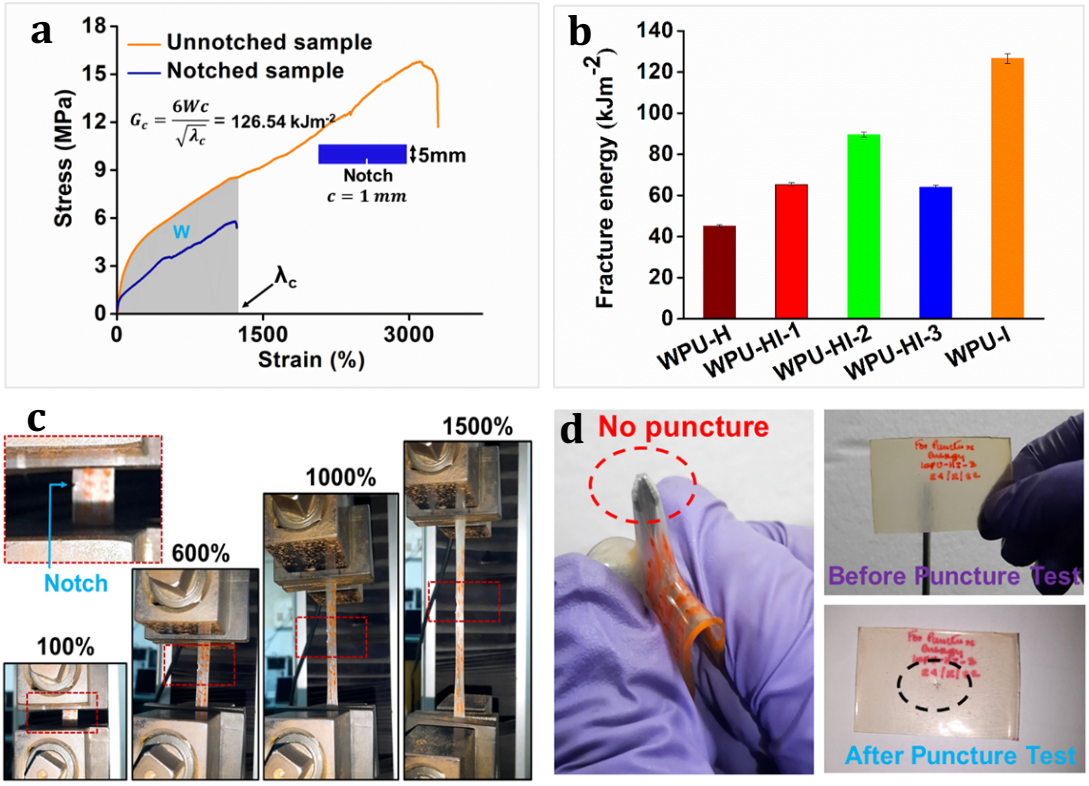

Figure 4.6. (a) Stress-strain profile of un-notched and notched WPU-I film, (b) fracture energy of all WPUs, (c) the process of fracture test for WPU-I, and (d) the puncture test on WPU-HI-3 (thickness of 0.8 mm) using a screw-driver with a tip of diameter 1.35 mm.

The fracture energy of WPU-HI-3 films was 63.93 kJm^{-2}, determined using Greensmith's method and the maximum value was 126.54 kJm^{-2} for WPU-I, which is also eye-catching among healable elastomers (**Figure 4.6 (a)** and **(b)**). Furthermore, a puncture test was also performed on WPU-HI-3 film using a screw-driver as shown in **Figure 4.6 (d)**. But we couldn't able to puncture the tested film even after three consecutive attempts which also supports the magnificent toughness. It can be claimed that there are three key factors that are assisting to accomplish the unprecedented toughness via physico-chemical crosslinking:

i) the considerably increased number of sacrificial H-bonds within the hard domains of WPU, ii) the rapid and reversible association/dissociation of hard domains with asymmetric IPDI-IPDA moieties, and iii) four branches of carbamate groups developed by each GECA [14].

4.3.4. Self-healing, shape memory, and re-processable performances

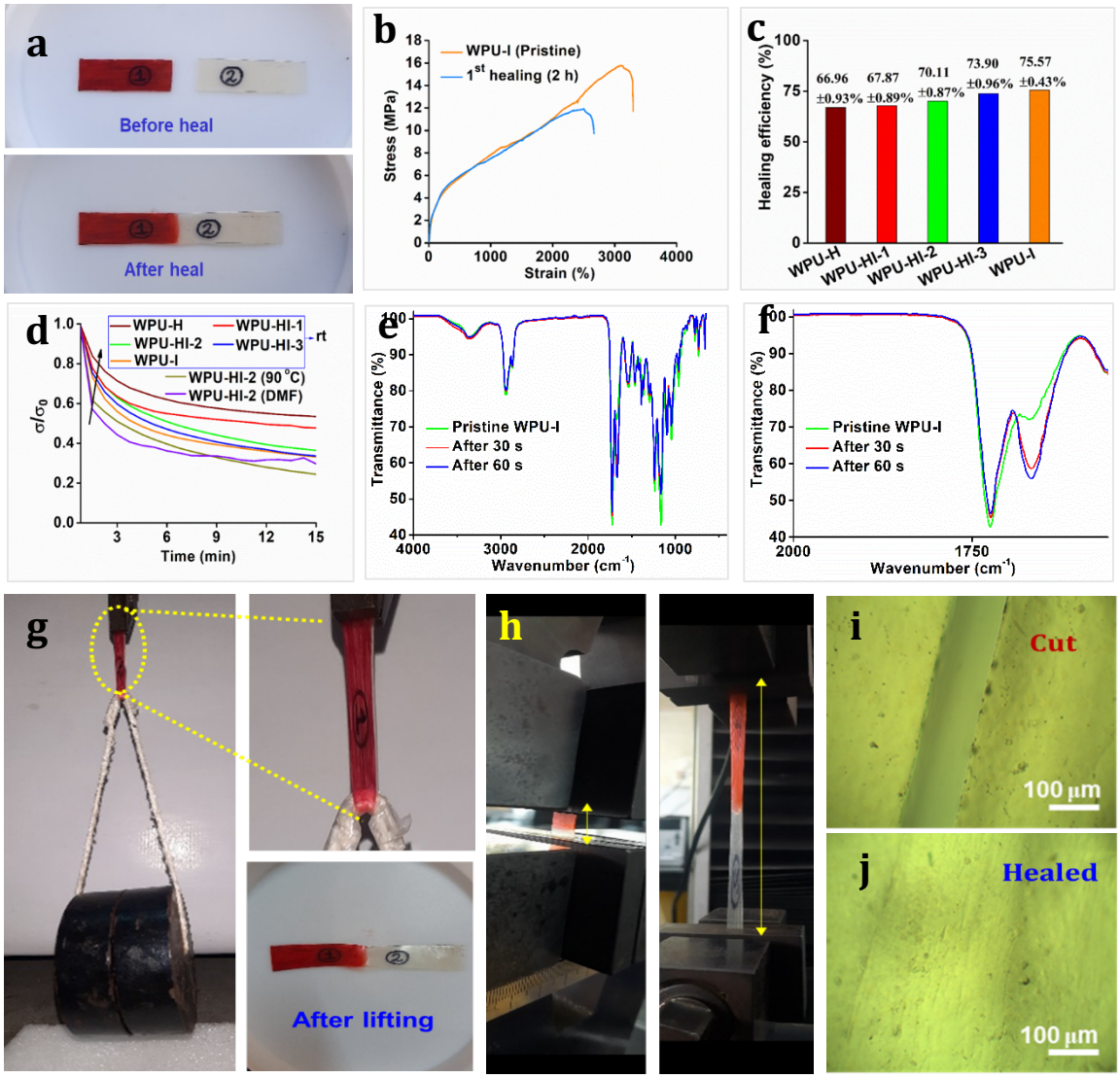

Figure 4.7. (a) No loss of structural integrity after spreading 0.2 μL of DMF on the surface of WPU-I, (b) stress-strain profiles of WPU-I before and after healing at 90 °C for 2 h, (c) percentage of healing efficiency of WPUs, (d) stress-relaxation curves of WPU films at two different temperatures (RT and 90 °C) and in presence of DMF, provided fixed strain of 10% for 15 min, (e-f) ATR spectra of the WPU-I specimen after being contacted with trace DMF, (g) weight lifting after healing (WPU-HI-2, 4 kg), (h) stretching test after healing, and (i-j) optical microscopic images of cut film and healed film of WPU-I.

In this report, the healing ability of WPU films was investigated quantitatively and qualitatively. It is familiar that the healing process is the combination of five stages: segmental surface rearrangement, surface approach, wetting, diffusion, and randomization

[24]. The most common stimuli that are used for intrinsic self-healing include sunlight, heat, microwave, electricity, etc. [25].

Earlier reports disclosed that trace solvent can also be used as a promising stimulus for healing polymeric materials by applying it to the identified damaged areas via spraying, coating, or spreading [26-27]. The usage of trace amounts of solvent will not cause major detriment to the environment. But it is pertinent to note that the trace solvent-induced healing process is not dependent on the dissolution effect. The intrinsic healing demands the recovery of the original shape, mechanical properties, and functionalities which is not possible in the dissolution technique as it requires more amount of solvent. The usage of a high amount of solvent will cause structural deformation, and decrement in the uniformity of the polymer, resulting in poor healing efficiency. So, in this report, we have used only 0.1-0.2 μL of DMF to re-join and heal the damaged WPU films. As shown in **Figure 4.7 (a),** this trace DMF spread on the damaged surface did not disturb the structural integrity (shape and size of the contact area) of the film tested. According to the previous report, the hard domains modified by asymmetric IPDA-IPDI moieties are insensitive to the moderate-high temperature (60-80 ℃) [14]. But high temperature enables the exchange of H-bonds within the hard domains. To evaluate the healing efficiency of WPUs elastomer, each WPU film was cut into two pieces and re-joined using 0.1-0.2 μL of DMF and healed under 90 ℃ at different times. For the comparative evaluation (**Figure 4.7 (b)** and **(c)** all films were healed at 90 ℃ for 2 h. It has been observed that all films were healed satisfactorily. The high healing ability can be attributed to the rapid and reversible rearrangement and reorganization of H-bonds within the WPU matrix. These manifestations facilitate suitable conditions for the re-combination of molecular chains and restore mechanical properties. However, results showed that healing efficiency increases with an increase in the amount of IPDI. The healing efficiency of WPU-H, WPU-HI-1, WPU-HI-2, WPU-HI-3, and WPU-I were 66.96%, 67.87%, 70.11%, 73.90%, and 75.57%, respectively. The main reason is that the IPDA-IPDI enables molecular chain mobility via the formation of loosely packed hard domains. Furthermore, the diffusion and randomization of polymer chains require sufficient time to repair the fractured surface and to form a new polymer network. So, the maximum healing efficiency can be attained via increasing self-healing time [28]. To realize the self-healing performance from rheology, the stress-relaxation experiment was conducted on the WPU films at RT and 90 ℃, provided at a fixed strain of 10% for 15 min. Additionally, to explore the key role of DMF in the healing mechanism, 0.2 μL DMF was spread on the film (WPU-HI-2) for 10 s prior to the test under the same condition. **Figure 4.7 (d)** shows that the relaxation time (λ) at RT increases in the order of WPU-I<WPU-HI-3<WPU-HI-2<WPU-HI-1<WPU-I which indicates

that the packing density of the hard domain is also increase in the same order [29]. Noticeably, the rate of relaxation accelerated when the temperature was raised to 90 °C and by the solvent treatment. This can be attributed to the increase in the chain mobility, resulting good healing efficiency via rapid exchange of H-bonds with IPDI-IPDA architecture. Again, the evolution of H-bonding was further investigated by attenuated total reflectance infrared (ATR-IR) after the fracture surface of WPU-I film was exposed to a small amount of DMF. As shown in **Figures 4.7 (e)** and **(f)**, it has been observed that the stretching frequency for –C=O (urea) at 1664 cm^{-1} exhibited an increasingly apparent red-shift with increasing contact time.

Table 4.2. Shape memory property of WPU films.

Parameters	WPU-H	WPU-HI -1	WPU-HI -2	WPU-HI -3	WPU-I
Shape fixity (%)	97.2	94.5	94.4	94.5	94.7
Shape recovery (%)	93.1	95.7	96.1	95.5	95.1
SR under heat (70 °C, water) (s)	55	53	48	46	40
SR under microwave radiation (900) W) (s)	210	200	180	180	120
Sunlight (h)	24	24	24	24	24

This result establishes that a tiny amount of DMF can help to amend the chain mobility and rearrangement in the hard domain which is mandatory for self-healing phenomenon [14]. For qualitative evaluation of healing, a weight-lifting test was performed by the healed film (WPU-HI-2) to establish good healing ability, as shown in **Figure 4.7 (g)**. It has been observed that the healed film can easily lift a weight of 4 kg without any damage. The stretchability of the healed film is shown in **Figure 4.7 (h)**. The optical microscopic images of unhealed and healed WPU-HI-2 films are shown in **Figure 4.7 (i)** and **(j),** showing that the cut mark slowly disappeared with time.

Again, the three most important parameters to assess the shape memory effect, namely, shape fixity (%), shape recovery (%), and recovery time were determined, and the results are summarized in **Table 4.2**. The digital images of shape memory behaviors of WPU film in the presence of warm water (70 °C) and microwave radiation (900 W) are shown in **Figures 4.8. (a-j)**. The shape memory elastomers are always associated with two primary attributes: a) "memory" of a stress-free permanent shape and b) "programming or fixing" of a temporary shape via the heating-deformation-cooling cycle [30]. At a molecular level, the memory is managed by a reversible phase (covalent or non-covalent crosslinks) established at a stress-free state during processing, while programming is achieved by kinetic trapping of a deformed and stressed shape i.e., fixation phase via crystallization, vitrification, crosslinking, or plastic deformation [31-32].

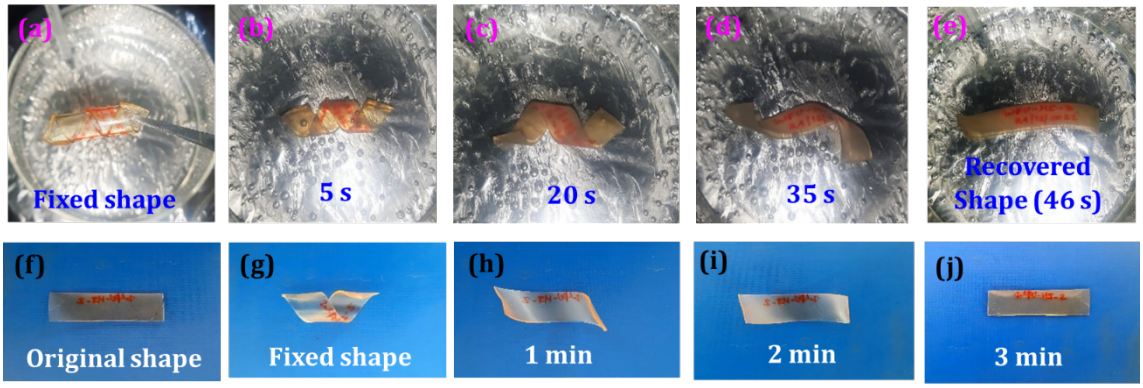

Figure 4.8. Shape memory test of WPU-HI-3 (a-e) under warm water at 70 °C and (f-i) WPU-HI-2 under microwave radiation (900W).

These molecular-level reversible transformations transfer to the molecular chain, resulting in macroscopic shape fixing. In this work, the semi-crystalline PCL (soft segment) served as the switching domains or fixation phase which controlled the fixing and recovering of temporary shape, while the hard segments i.e., urea and urethane linkages (hard segment) served as the reversible phase. When the WPU films were heated above the glass transition temperature of the hard segment, Brownian motion developed among the polymeric chain. At this fragile moment when entropy is maximum, the WPU can be deformed and shaped by applying an external force. Then, rapid cooling of the deformed structure restricted the chain mobility and decrease the entropy of the WPU which is also supported by the semi-crystallinity of PCL, H-bonding, and branched structure of GECA. The P-XRD showed that the crystallinity decreases from WPU-H to WPU-I and so the shape fixity (**Table 4.2**). Subsequently, reheating the WPU films above glass transition temperature help to re-mobilize the molecular chain, resulting increase in the entropy of branched architecture of GECA. Additionally, the residual strain, stored in the WPU matrix during shape fixation boost

the shape recovery. So, the shape recovery time is minimum for WPU-I that exhibited the maximum elastic strain energy with high chemical cross-linking.

Finally, the physical reprocessing of the WPU films used in various test was performed as follows: films were cut into small pieces (about 3×3 mm^2) and then hot-press in a compression molding machine at 60 °C under 60-80 $kgcm^{-2}$ pressure for 30 minutes (**Figure 4.9 (a)**). The mechanical properties and thermal stabilities of WPUs were evaluated after reprocessing. Results showed that the good thermal stability retained or even a marginal increase in stability after reprocessing was noticed near 230-300 °C (**Figure 4.9 (b)**).

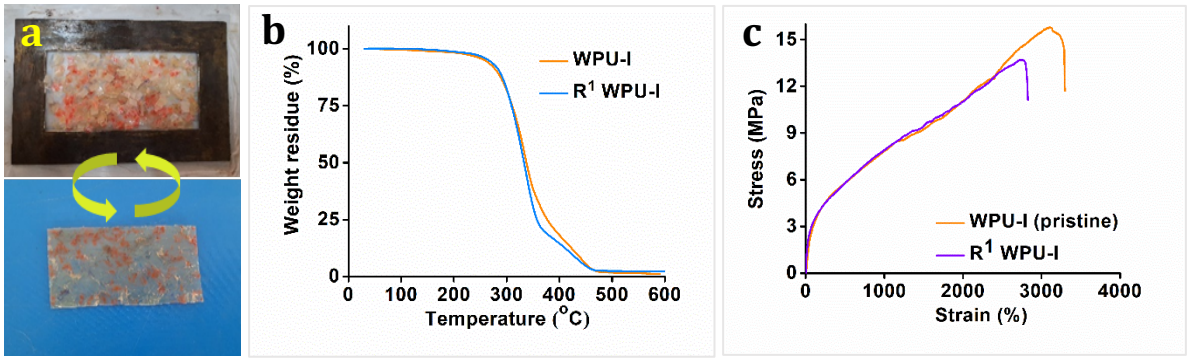

Figure 4.9. (a) Small pieces of used films and a reprocessed film, (b) TGA thermograms, and (c) stress-strain profiles of pristine WPU-I and reprocessed WPU-I (R^1-WPU) films (recovery efficiency- stress of 86.94% & strain of 85.77%).

But tensile stress and strain slightly decreased to 13.78 MPa and 2828%, respectively (**Figure 4.9 (c)**), because of locking of air-bubble inside the film during compression. Otherwise, mechanical properties can also be retained with 100% reprocessing efficiency, repeatedly. So, it can be claimed that the WPU films can be self-repairable and recyclable, prolonging its service life which will surely reduce environmental pollution with high sustainability.

4.3.5. Hemocompatibility assay of WPU films

Clinically applicable materials are poised to possess minimal or no platelet adhesion activity, as it could lead to the induction of severe thrombogenesis and the formation of atherosclerotic plaque [17]. Here, the modified PU, i.e., WPU films showed minimal adhesion of platelets as compared to the collagen-coated positive controls which could be observed in the rhodamine-phalloidin stained fluorescent micrographs (**Figure 4.10 (a)**). Platelets were found to have sparsely adhered to the WPU films. The adhered platelets were additionally assessed for their activity using LDH assay. The platelets adhered to collagen-coated surfaces

showed higher LDH activity ($p \leq 0.05$) as compared to the platelets adhered to the WPU films (**Figure 4.10 (b)**). These results were in accordance with previously conducted studies on PU-derived materials [18-19]. The WPU films showed comparable LDH activity in all the groups and could be considered antithrombogenic. Further, RBC lysis assay was conducted to determine the whole blood compatibility of the various WPU variants. The assay indicated minimal lysis of RBCs when they were kept in contact with the WPU disks (**Figure 4.10 (c)**). The supernatant derived after incubation with WPU films had comparable absorbance to the 150 mM NaCl buffer, i.e., the negative control, and was significantly lesser than 20% TritonX-100, the positive control ($p \leq 0.01$). These results affirmed the overall hemocompatibility of the various WPU films proving them suitable for the development of stent and suture materials.

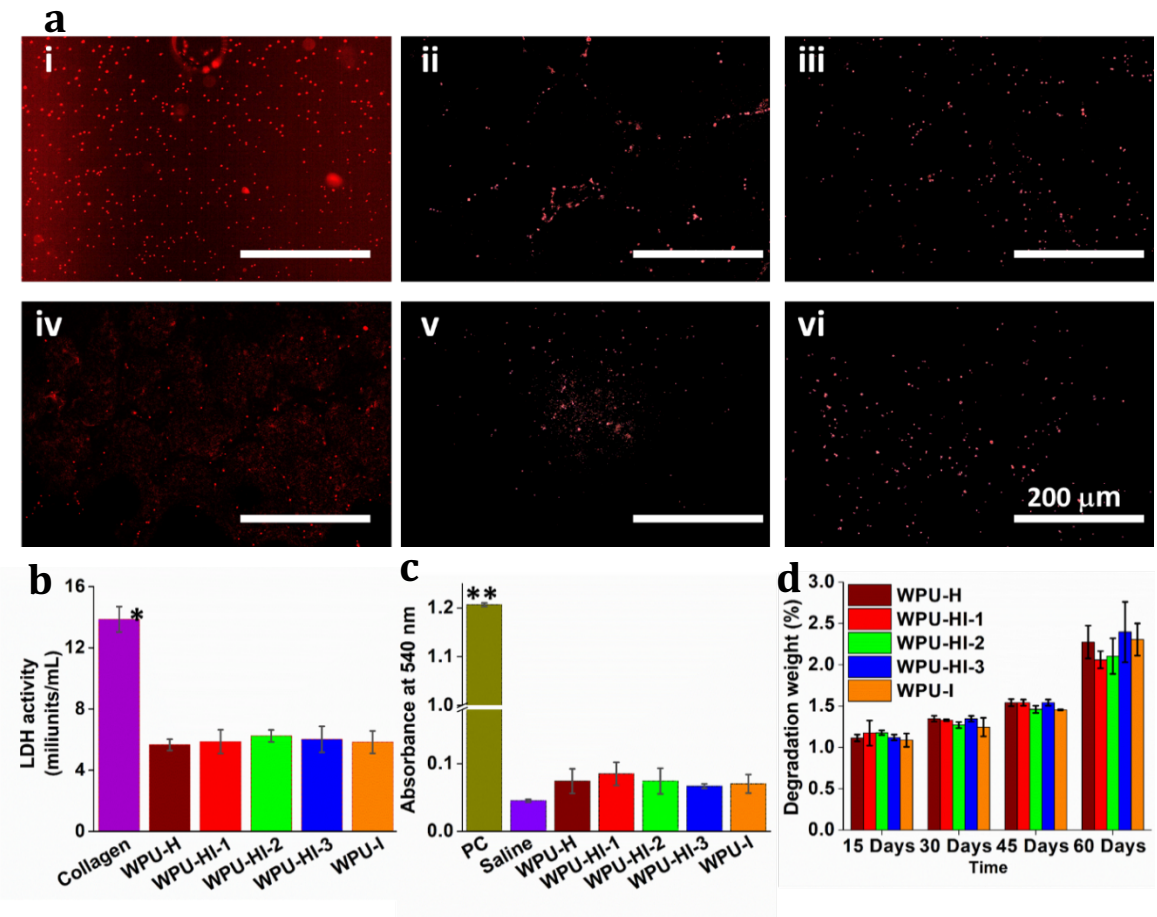

Figure 4.10. (a) Representative rhodamine-phalloidin stained micrographs of platelets adherance on (i) collagen coated surface, (ii) WPU-H, (iii) WPU-HI-1, (iv) WPU-HI-2, (v) WPU-HI-3, and (vi) WPU-I, b) LDH activity of the platelets adhered on the various WPU surfaces as compared with collagen as positive control, (c) RBC lysis caused by PC (20% Triton-X 100), Saline (150mM NaCl) and various WPU surfaces measured optically, and (d) degradation of various films on days 15, 30, 45 and 60 days incubated in 0.1M PBS expressed as weight percentage degraded. (n=3, *$p \leq 0.05$ and **$p \leq 0.001$, scale bar: 200 µm).

4.3.6. *In vitro* degradation study

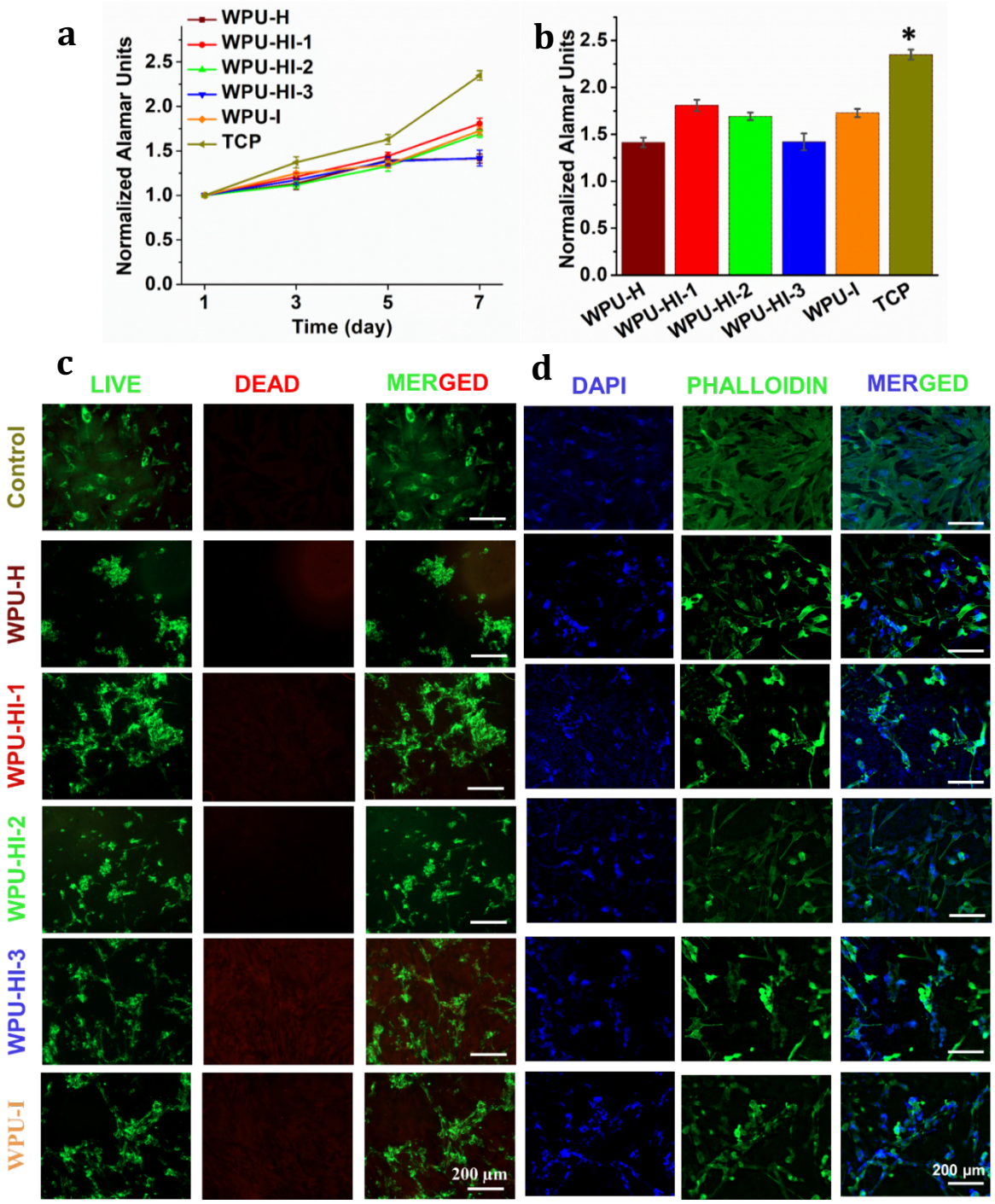

Figure 4.11. (a) Alamar blue based cellular proliferation of HDF seeded on various WPU surfaces and TCP (Tissue Culture Plate), (b) reduced alamar units on day 7 depicting the variation in proliferation of HDF on various surfaces. (n=4, *p≤0.05), (c) representative micrographs showing live-dead imaging after 7 days of incubation in Control (Tissue Culture Dish) and WPUs, and (d) representative micrographs showing phalloidin-DAPI imaging after 7 days of incubation in Control (Tissue Culture Dish) and WPUs showing the cytoskeleton and the nuclei (scale bar: 200 µm).

The WPU films of various types were found to undergo minimal degradation and weight loss of ≤ 3% in all of the cases over the period of 60 days (**Figure 4.10 (d)**). This is in concurrence with the results of previously observed PU composite materials [18]. This

minimal loss of weight indicates the long term stability of the WPU material and touts its subsequent use in vivo. Further, the actual degradability of the material needs to be evaluated in vivo which will be influenced by the interaction of the WPU elastomer variants with the body fluids.

4.3.7. Cellular viability and proliferation

Higher reduction of Alamar blue could be directly correlated to the enhanced metabolic activity and proliferation of the cells. HDFs were found to proliferate >1.5 times when seeded on WPU-HI-1, WPU-HI-2 and WPU-I, while the cells seeded on WPU-H and WPU-HI-3 showed slightly less than 1.5 times proliferation (**Figure 4.11 (a)**). All of the groups showed significantly lower proliferation ($p \leq 0.05$) as compared to the TCP control which showed > 2 times of proliferation (**Figure 4.11 (b)**). Cells were observed after 7 days of culture on various surfaces using live/dead assay. The live cells (stained with green fluorescence) were found to adhere and spread on the TCP (**Figure 4.11 (c)**) while the live cells on various WPU surfaces showed spread as well as rounded morphologies. The cells were found to grow in aggregates over the WPU films as compared to the TCP controls as observed after 7 days. Furthermore, as shown in **Figure 4.11 (d)**, we have acquired a set of cytoskeleton (phalloidin) and nucleus (DAPI) stained images for the various WPU substrates. These images could hence depict the morphological changes in the cells due to the presence of WPU with clustered cells on the PU substrates as compared to the spread morphology on the cell culture plate. Hence, the cellular viability and proliferation corroborated the biocompatibility of the WPU films and their ability to support cellular adhesion as well as proliferation under in vitro conditions.

4.3.8. Biodegradation of WPU films

To establish the environment friendly nature of the WPUs even after its service period, biodegradation was studied by using gram-positive bacteria like *B. subtilis* which has high possibility of availability in soil. The change in the optical density (OD) of the bacterial solution where WPUs films were immerged and weight loss after two months of biodegradation test were determined **(Figure 4.12 (a)** and **(b)**. It has been observed that the bacterial growth on WPU film is satisfactory. SEM image of degraded film and its respective 3D surface plot (**Figure 4.12 (c)** and **(d)** confirmed the acceptable biodegradation of WPU-HI-2 film. Bacteria, especially attack on the easily hydrolysable group such as ester moiety present in the WPU matrix. Previously, Howard and Rowe also reported that *B. subtilis* can be growth in PU matrix [33]. After the test, it has been observed that the less crystalline WPU-

I showed better degradation than more crystalline WPU-H. A similar result has been reported by Huang and Robay [34]. Thus, the newly synthesized biobased WPU elastomers will not harm the environment like non-biodegradable commercially available polymer after its service life.

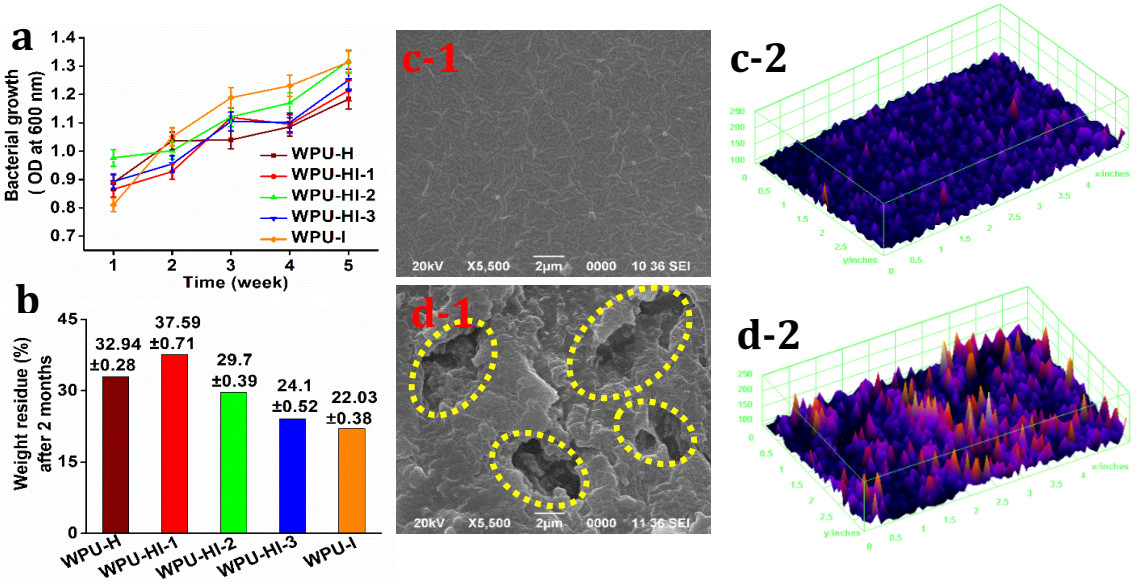

Figure 4.12. (a) Change in the optical density (OD) of the *B. subtilis* bacterial solution with WPU films, (b) weight residue after 2 months of microbial exposure; SEM images of (c-1) controlled (before biodegradation) and (d-1) biodegraded of WPU-HI-2 film, and (c-2 and (d-2) surface 3D plots of SEM images obtained from ImageJ software.

4.4 Conclusion

In conclusion, we have designed a facile strategy to prepare an environmentally benign self-healable WPU exhibiting high mechanical strength, unprecedented toughness, shape recovery, superb fracture resistant, and extreme stretchability. To address the paradoxical relationship between mechanical strength and healing efficiency, we have introduced the high-density hindered urea-based hydrogen bonds, asymmetric alicyclic rings i.e., IPDI-IPDA architecture, and GECA, (internal emulsifier) into the hard domains of WPU. A trace amount solvent and the loosely packed asymmetric moieties facilitate the molecular chain mobility to achieve good healing efficiency under mild conditions. Interestingly, biological assessment unveiled that all WPU films demonstrated hemocompatibility and cytocompability along with desired biodegradability. So, we believe that the resultant WPU elastomers can be used as smart biomaterials and coatings for biomedical devices. For example, it can be directly used as a minimally invasive smart suture. WPU elastomer can also be used as an artificial muscle by taking advantage of its good shape fixity and recovery rate. Furthermore, the WPU dispersion can be post-modified with a biocompatible cross-linker such as gelatin for preparing ink which can be used in 3D-bioprinting.

References

[1] Delebecq, E., Pascault, J. P., Boutevin, B. and Ganachaud, F. On the versatility of urethane/urea bonds: reversibility, blocked isocyanate, and non-isocyanate polyurethane. *Chemical Reviews*, 113(1):80-118, 2013.

[2] Priemel, T., Degtyar, E., Dean, M. N. and Harrington, M. J. Rapid self-assembly of complex biomolecular architectures during mussel byssus biofabrication. *Nature Communications*, 8(1):14539, 2017.

[3] Yoshida, S., Ejima, H. and Yoshie, N. Tough elastomers with superior self-recoverability induced by bioinspired multiphase design. *Advanced Functional Materials*, 27(30):1701670, 2017.

[4] Zhang, H. J., Sun, T. L., Zhang, A. K., Ikura, Y., Nakajima, T., Nonoyama, T., Kurokawa, T., Ito, O., Ishitobi, H. and Gong, J. P. Tough physical double-network hydrogels based on amphiphilic triblock copolymers. *Advanced Materials*, 28(24):4884-4890, 2016.

[5] Wu, J., Cai, L. H. and Weitz, D. A. Tough self-healing elastomers by molecular enforced integration of covalent and reversible networks. *Advanced Materials*, 29(38):1702616, 2017.

[6] Burnworth, M., Tang, L., Kumpfer, J. R., Duncan, A. J., Beyer, F. L., Fiore, G. L., Rowan, S. J. and Weder, C. Optically healable supramolecular polymers. *Nature*, 472(7343):334-337, 2011.

[7] Liu, J., Tan, C. S. Y., Yu, Z., Li, N., Abell, C. and Scherman, O. A. Tough supramolecular polymer networks with extreme stretchability and fast room-temperature self-healing. *Advanced Materials*, 29(22):1605325, 2017.

[8] Liu, Y. L. and Chuo, T. W. Self-healing polymers based on thermally reversible Diels–Alder chemistry. *Polymer Chemistry*, 4(7):2194-2205, 2013.

[9] Imato, K., Takahara, A. and Otsuka, H. Self-healing of a cross-linked polymer with dynamic covalent linkages at mild temperature and evaluation at macroscopic and molecular levels. *Macromolecules*, 48(16):5632-5639, 2015.

[10] Ying, H. and Cheng, J. Hydrolyzable polyureas bearing hindered urea bonds. *Journal of the American Chemical Society*, 136(49):16974-16977, 2014.

[11] Lu, Y. X. and Guan, Z. Olefin metathesis for effective polymer healing via dynamic exchange of strong carbon–carbon double bonds. *Journal of the American Chemical Society*, 134(34):14226-14231, 2012.

[12] Cromwell, O. R., Chung, J. and Guan, Z. Malleable and self-healing covalent polymer networks through tunable dynamic boronic ester bonds. *Journal of the American Chemical Society*, 137(20):6492-6495, 2015.

[13] Song, P. and Wang, H. High-performance polymeric materials through hydrogen-bond cross-linking. *Advanced Materials*, 32(18):1901244, 2020.

[14] Wang, D., Wang, Z., Ren, S., Xu, J., Wang, C., Hu, P. and Fu, J. Molecular engineering of a colorless, extremely tough, superiorly self-recoverable, and healable poly (urethane–urea) elastomer for impact-resistant applications. *Materials Horizons*, 8(8):2238-2250, 2021.

[15] Greensmith, H. W. Rupture of rubber. X. The change in stored energy on making a small cut in a test piece held in simple extension. *Journal of Applied Polymer Science*, 7(3):993-1002, 1963.

[16] Liu, T., Li, C., Yao, H., Sun, F., Wang, L., Yao, B., Xu, J. and Fu, J. Extremely strengthening fatigue resistance, elastic restorability and thermodynamic stability of a soft transparent self-healing network based on a dynamic molecular confinement-induced bioinspired nanostructure. *Materials Horizons*, 10:2968-2979, 2023.

[17] Duarah, R., Singh, Y. P., Gupta, P., Mandal, B. B. and Karak, N. High performance bio-based hyperbranched polyurethane/carbon dot-silver nanocomposite: a rapid self-expandable stent. *Biofabrication*, 8(4):045013, 2016.

[18] Duarah, R., Singh, Y. P., Mandal, B. B. and Karak, N. Sustainable starch modified polyol based tough, biocompatible, hyperbranched polyurethane with a shape memory attribute. *New Journal of Chemistry*, 40(6):5152-5163, 2016.

[19] Duarah, R., Singh, Y. P., Gupta, P., Mandal, B. B. and Karak, N. Smart self-tightening surgical suture from a tough bio-based hyperbranched polyurethane/reduced carbon dot nanocomposite. *Biomedical Materials*, 13(4):045004, 2018.

[20] Morang, S., Biswakarma, N., Deka, R. C. and Karak, N. Citric acid/glycerol ester, a backup of 2, 2-bis (hydroxymethyl) propionic acid and biobased synthesis of anionic polyurethane dispersion. *Progress in Organic Coatings*, 168:106880, 2022.

[21] Wang, D., Xu, J., Chen, J., Hu, P., Wang, Y., Jiang, W. and Fu, J. Transparent, mechanically strong, extremely tough, self-recoverable, healable supramolecular elastomers facilely fabricated via dynamic hard domains design for multifunctional applications. *Advanced Functional Materials*, 30(3):1907109, 2020.

[22] Shi, C. Y., Zhang, Q., Yu, C. Y., Rao, S. J., Yang, S., Tian, H. and Qu, D. H. An ultrastrong and highly stretchable polyurethane elastomer enabled by a zipper-like ring-sliding effect. *Advanced Materials*, 32(23):2000345, 2020.

[23] Li, Y., Li, W., Sun, A., Jing, M., Liu, X., Wei, L., Wu, K. and Fu, Q. A self-reinforcing and self-healing elastomer with high strength, unprecedented toughness and room-temperature reparability. *Materials Horizons*, 8(1):267-275, 2021.

[24] Ghosh, B. and Urban, M. W. Self-repairing oxetane-substituted chitosan polyurethane networks. *Science*, 323(5920):1458-1460, 2009.

[25] Eom, Y., Kim, S. M., Lee, M., Jeon, H., Park, J., Lee, E. S., Hwang, S. Y., Park, J. and Oh, D. X. Mechano-responsive hydrogen-bonding array of thermoplastic polyurethane elastomer captures both strength and self-healing. *Nature Communications*, 12(1):621, 2021.

[26] Yang, Y., Terentjev, E. M., Wei, Y. and Ji, Y. Solvent-assisted programming of flat polymer sheets into reconfigurable and self-healing 3D structures. *Nature Communications*, 9(1):1906, 2018.

[27] Ravi, B., Mukherjee, R. and Bandyopadhyay, D. Solvent vapour mediated spontaneous healing of self-organized defects of liquid crystal films. *Soft Matter*, 11(1):139-146, 2015.

[28] Jing, T., Heng, X., Guifeng, X., Ling, C., Pingyun, L. and Xiaode, G. Highly stretchable, high efficiency room temperature self-healing polyurethane adhesive based on hydrogen bonds–applicable to solid rocket propellants. *Polymer Chemistry*, 12(31):4532-4545, 2021.

[29] Kim, S. M., Jeon, H., Shin, S. H., Park, S. A., Jegal, J., Hwang, S. Y., Oh, D. X. and Park, J. Superior toughness and fast self-healing at room temperature engineered by transparent elastomers. *Advanced Materials*, 30(1):1705145, 2018.

[30] Lendlein, A. and Kelch, S. Shape-memory polymers. *Angewandte Chemie International Edition*, 41(12):2034-2057, 2002.

[31] Ur Rehman, H., Chen, Y., Hedenqvist, M. S., Li, H., Xue, W., Guo, Y., Guo, Y., Duan, H. and Liu, H. Self-healing shape memory PUPCL copolymer with high cycle life. *Advanced Functional Materials*, 28(7):1704109, 2018.

[32] Penfold, N. J., Yeow, J., Boyer, C. and Armes, S. P. Emerging trends in polymerization-induced self-assembly. *ACS Macro Letters*, 8(8):1029-1054, 2019.

[33] Rowe, L. and Howard, G. T. Growth of Bacillus subtilis on polyurethane and the purification and characterization of a polyurethanase-lipase enzyme. *International Biodeterioration & Biodegradation*, 50(1):33-40, 2002.

[34] Huang, S. J. and Roby, M. S. Biodegradable polymers poly(amide-urethanes). *Journal of Bioactive and Compatible Polymers*, 1(1):61-71, 1986.